1-1-2016

Novel Cell Penetrating Peptide-adaptors Effect Intracellular Delivery and Endosomal Escape of Protein Cargos

John C. Salerno
Kennesaw State University, jsalern3@kennesaw.edu

Verra M. Ngwa
Kennesaw State University

Scott J. Nowak
Kennesaw State University, snowak@kennesaw.edu

Carol A. Chrestensen
Kennesaw State University, cchreste@kennesaw.edu

Allison N. Healey
New Echota Biotechnology

See next page for additional authors

Novel cell penetrating peptide-adaptors effect intracellular delivery and endosomal escape of protein cargos

John C. Salerno,[1‡] Verra M. Ngwa,[2] Scott J. Nowak,[1] Carol A. Chrestensen,[2] Allison N. Healey[3] and Jonathan L. McMurry[1*]

Departments of [1]Molecular & Cellular Biology and [2]Chemistry & Biochemistry, Kennesaw State University, Kennesaw, GA 30144; [3]New Echota Biotechnology, Kennesaw, GA

Requests and inquiries to: Jonathan McMurry, Dept. Molecular & Cellular Biology, Kennesaw State University, 370 Paulding Ave. NW, MD#1201, Kennesaw, GA 30144; jmcmurr1@kennesaw.edu, 470-578-3238

Keywords: cell penetrating peptides, protein transduction domains, TAT, confocal microscopy, cellular delivery, protein transport

SUMMARY STATEMENT

Novel cell penetrating peptide-calmodulin adaptor proteins effect efficient delivery of user-defined cargo proteins to the cytoplasms of living mammalian cells.

‡ John Salerno passed away on Dec. 25, 2015.

ABSTRACT

The use of cell penetrating peptides (CPPs) as biomolecular delivery vehicles holds great promise for therapeutic and other applications, but development has been stymied by poor delivery and lack of endosomal escape. We have developed a CPP-adaptor system capable of efficient intracellular delivery and endosomal escape of user-defined protein cargos. The cell penetrating sequence of HIV transactivator of transcription was fused to calmodulin, which binds with subnanomolar affinity to proteins containing a calmodulin binding site. Our strategy has tremendous advantage over prior CPP technologies because it utilizes high affinity noncovalent, but reversible coupling between CPP and cargo. Three different cargo proteins fused to a calmodulin binding sequence were delivered to the cytoplasm of eukaryotic cells and released, demonstrating the feasibility of numerous applications in living cells including alteration of signaling pathways and gene expression.

INTRODUCTION

In recent years a number of peptides that are rapidly internalized by mammalian cells have been discovered or designed (Fonseca, et al., 2009; Sebbage, 2009; Johnson, et al., 2011). Cell-penetrating peptides (CPPs) are capable of mediating penetration of the plasma membrane, allowing delivery of macromolecular cargos to which they are attached to cell interiors. CPPs are typically 10 to 30 amino acids long and fall into one of three major categories: arginine-rich, amphipathic and lysine-rich, and hydrophobic (Gautam, et al., 2012). CPP delivery of cargos to the interior compartments of cells is potentially transformative as a research tool, diagnostic aid and therapeutic mechanism.

More than 25 CPP clinical trials are underway, including a Phase III (Glogau, et al., 2012; Lonn and Dowdy, 2015). However, CPPs have largely disappointed (Palm-Apergi, et al., 2012) for a variety of reasons including nonpenetration (Lundberg, et al., 2003), limited endosomal escape (Erazo-Oliveras, et al., 2012), and requirements for hydrophobic cargos (Hirose, et al., 2012). Described CPP technologies are reliant on covalent crosslinking or nonspecific hydrophobic interactions (Koren and Torchilin, 2012).

The work described herein describes a novel technology that solves or ameliorates all of these problems. We have designed a CPP-adaptor fusion protein, TAT-Calmodulin (TAT-CaM), which noncovalently binds, delivers and releases cargo into the cytoplasm. Three different cargo proteins were chosen to reflect a range of characteristics including size, oligomerization and structure. The strategy is generally applicable to any soluble protein and may also be used to deliver nonprotein cargos such as RNA. Assays can be performed in real time with live cells without significant cytotoxicity and offers an alternative to transfection. Our advance greatly expands the applications and effectiveness of CPPs.

RESULTS & DISCUSSION

Schematics of the CPP-adaptor and cargo proteins are shown in Fig. 1A. Our prototype CPP-adaptor, TAT-CaM, consists of the cell penetrating sequence from the HIV transactivator of transcription (Green and Lowenstein, 1988) fused to calmodulin (CaM). Calmodulin was selected as the prototype adaptor not only because it binds its partners with high affinity in the presence of calcium, but also because mammalian cells typically maintain low resting cytoplasmic Ca^{2+} levels, allowing rapid release of cargo after internalization as affinity of CaM for its ligands is negligible in the absence of Ca^{2+}. Cargos are fused to a N-terminal CaM binding sequence (CBS) encoded by the vector.

The affinity of TAT-CaM for a natural ligand was first examined. TAT-CaM bound to neuronal nitric oxide synthase (nNOS) via the native CaM binding site with affinity similar to wild-type CaM as assayed with biolayer interferometry (BLI), an optical biosensing technique similar to surface plasmon resonance (Fig. 1B) (Abdiche, et al., 2008; Sultana and Lee, 2015; McMurry, et al., 2011). Model cargos were then examined for CaM binding affinity and kinetics. Cargos myoglobin (CBS-Myo), horse radish peroxidase (CBS-HRP) and β-galactosidase (CBS-β-Gal) all bound CaM with low nanomolar affinity and expected fast-on, slow off kinetics (Fig. 1C-E). TAT-CaM and cargo proteins dissociated rapidly upon exposure to EDTA (k_{off} ~ 0.1 s^{-1}, Fig. 1F), indicating that the TAT-CaM-CBS interactions function essentially indistinguishably from those of wild type CaM. All analytes exhibited negligible binding to sensors without TAT-CaM. Rate and affinity constants determined from single-state global fits are listed in Table 1.

1 μM each of TAT-CaM and fluorescently-labelled cargo protein in buffer containing 1 mM $CaCl_2$ were added to subconfluent BHK21 cells and incubated for 1 hour, after which cells were washed and imaged by fluorescence confocal microscopy. Uptake of cargo into cell interiors was assayed using an inverted Zeiss (Jena, Germany) LSM700 confocal microscope equipped with a 40x EC Plan-Neofluar objective (NA= 1.3). Z-stacks of both TAT-CaM treated and untreated cells

were acquired and analyzed for incorporation of fluorescently labeled cargo into the cytoplasm. Orthogonal projections of Z-stacks were generated using Zeiss ZEN software, which allowed for viewing both treated and untreated cells alike at the same depth within the cell relative to the diameter of the nucleus. As shown in Fig. 2, all cargo proteins were delivered to the interiors of the cells and showed significant cytoplasmic distribution, indicating efficient penetration and escape from endosomes. The fluorescently labelled cargo proteins without TAT-CaM showed a very small degree of adherence to the surfaces of cells, but no penetration into the cell as observed by absence of fluorescence at the same cytoplasmic depth as that observed in cells treated with TAT-CaM (Fig 2A-C). Cargos reflect an array of characteristics, e.g. myoglobin is small, all-alpha helical and monomeric while β-galactosidase is large, structurally complex and forms a 464 kDa tetramer (Jacobson, Zhangand, 1994). TAT-CaM delivers all cargos yet examined, including nNOS (data not shown).

To demonstrate broad utility of cargo uptake in different types of cells, subconfluent HEK and HT-3 cells were treated with CBS-myoglobin cargo under identical conditions, and assayed using the same conditions as above (Figure 3). HT-3 is a human retinoblastoma line of cervical type cells and HEK cells are human, embryonic and have an epithelial morphology whereas BHK cells have fibroblast morphology. As observed with BHK cells, CBS-myoglobin was also delivered to the interior of these different mammalian cell lines, indicating that cargo delivery can occur regardless of cell type used.

Other CPP-cargo strategies rely on covalent linkage or nonspecific hydrophobic linkers that are susceptible to getting trapped by membrane association as the CPP itself may not be released into the cytoplasm. Even non-hydrophobic CPPs are likely to be tightly bound to membrane proteins involved in endocytosis or transmembrane translocation, which would be expected to greatly hinder endosomal escape by covalently attached cargo proteins. One group estimates that a fraction of 1% of TAT-fused cargos escape endosomes (Lonn and Dowdy, 2015).

Our strategy of high-affinity but reversible noncovalent attachment of cargos overcomes trapping effects via Ca^{2+}-dependent dissociation, allowing rapid and efficient cargo distribution to the cytoplasm even though TAT may remain trapped in the endosome.

Cytotoxicity is also a major drawback with current CPPs, particularly given the concentrations necessary to attain observable endosomal escape. Cytotoxic effects of TAT become significant in the tens of μM (Cardozo, et al., 2007). That TAT-CaM effects significant cytoplasmic distribution of cargos at 1 μM without an increase in cell death as measured by Trypan Blue exclusion (data not shown) is particularly exciting.

The time frame of cargo delivery using CPP-adaptors is under an hour, and likely much faster. This is in stark contrast to the time needed to transfect cells; CPP-adaptor delivery is roughly two orders of magnitude faster than transfection, making possible time course experiments that could not previously be attempted.

The array of applications made possible by our method is vast. For example, CPP-adaptors can be developed that allow for subcellular addressing, e.g. delivery of a transcription factor to the nucleus. Delivery of antibodies, enzymes, nucleic acids and small molecules are all potentially transformative methods. Follow-up studies to address kinetics, dosing, toxicity and other parameters as well as delivery of a wide array of cargos are underway.

MATERIALS & METHODS

Expression and purification. Our prototype CPP-adaptor, TAT-CaM, (New Echota Biotechnology, Kennesaw, GA, USA), is encoded by a pET19b-based vector containing a cleavable His-tag, the cell penetrating sequence from the HIV transactivator of transcription (Green and Lowenstein, 1988) fused to calmodulin via a GGR linker. TAT-CaM was expressed and purified from *E. coli* BL21(DE3)pLysS using metal affinity chromatography essentially as described (McMurry, et al., 2015). Cargo proteins were expressed in BL21(DE3)pLysS from synthetic, *E. coli* optimized genes cloned into pCal-N-FLAG-based plasmids (Agilent Technologies, CA, USA), which contain vector-encoded N-terminal calmodulin binding sequences. Cargos were purified to near homogeneity using a calmodulin sepharose column (GE Life Sciences, Pittsburgh, PA, USA) and dialyzed into binding buffer (10 mM HEPES, pH 7.4, 150 mM NaCl, 10% glycerol, 1 mM $CaCl_2$, 1 mM DTT). Cargos were myoglobin (CBS-Myo, from Accession #AH002877), horse radish peroxidase (CBS-HRP, E01651) and β-galactosidase (CBS-β-Gal, M22590). Neuronal nitric oxide synthase was expressed and purified as described (Gerber, et al.. 1995; Roman, et al., 1995) and exchanged into binding buffer as above. For cell penetration assays, cargo proteins were labelled with DyLight 550 (Thermo Fisher, USA) according to the manufacturer's protocol. Unreacted label was removed via a dye binding column.

Biolayer interferometry. BLI experiments were performed using a FortéBio (Menlo Park, CA, USA) Octet QK using SA sensors. Assays were done in 96 well plates at 25^0 C. 200µL volumes were used in each well. Ligands were loaded onto sensors for 300-900 s followed by baseline measurements in binding buffer for 300 s. Association was measured by dipping sensors into solutions of analyte protein and was followed by moving sensors to buffer only to monitor dissociation. Binding was fit to a global 1:1 association-then-dissociation model using GraphPad Prism 5.02.

Cell penetration assays. 1 µM each of TAT-CaM and DyLight 550-labelled cargo protein in binding buffer were added to subconfluent BHK21 (authenticated line purchased from ATCC (#CCL-10) in 2010; frozen aliquots were expanded for assays), human embryonic kidney (HEK, gift from David Fulton, Medical College of Georgia) or HT-3 (purchased in 2015 from ATCC, #HTB-32) cells and incubated for 1 hour, after which cells were washed three times in phosphate buffered saline with 1 mM $CaCl_2$. Following treatment with 2µM CellTracker Green CMFDA Dye (ThermoFisher) to label the cytoplasmic compartment, cells were labelled with NucBlue (ThermoFisher) and transferred to media containing 25 mM HEPES, pH 7.4 for imaging. Cells were immediately imaged on an inverted Zeiss LSM700 Confocal Microscope equipped with a 40x EC Plan-Neofluar objective (NA=1.3). Pinholes for each fluorophore were set at 1.0 Airy Units (29 microns). SP 490 and LP 615 filters were used to acquire the NucBlue (Blue channel) and DyLight 550 (Red Channel) signals, respectively. CellTracker Green signal (Green channel) was acquired using a BP 490-555 filter. Filters were carefully chosen to minimize spectral overlap between DyLight and CellTracker Green signals at the expense of some decline in signal quality.

Z-stacks for both TaT-CaM- treated and untreated cells were set by using the NucBlue staining of the nucleus as a reference (typical Z-stacks ranged from 6.0-10.0 microns). Both treated and untreated cells were imaged at identical gain settings, set at sub-saturation levels on cells treated with TaT-CaM in the red emission (DyLight 550 fluorescence). Both treated and untreated cells were imaged at an identical laser output level (2.0%, 555 nm laser), identical pixel dwell time of 3.15 microseconds, and 2x line averaging.

For analysis, images were rendered using the Orthogonal View in Zen Blue (Zeiss) software. Using the diameter of the nucleus as a landmark, the Z-plane chosen for analysis corresponded to approximately the mid-point depth of the nucleus. The DyLight 550 signal was analyzed separately (Figures 2 and 3, left panel, white signal), and merged with NucBlue (Figure 2, right panel, red (DyLight 550) and white (NucBlue), respectively). Finally, CellTracker Green

channel was included to aid in visualization of the cytoplasmic compartment in treated and untreated cells.

Competing Interests Statement

McMurry and Salerno have equity interest in New Echota Biotechnology, which has exclusive license to a pending patent on the described CPP-adaptor technology and a provisional patent on downstream applications. The other authors have no competing interests.

Author Contributions

John Salerno conceived of TAT-CaM and contributed to design and analysis of experiments. Verra Ngwa conducted many of the experiments, designed the cargos and helped write the manuscript. Scott Nowak performed the confocal microscopy. Carol Chrestensen performed tissue culture work. Nowak and Chrestensen consulted on experimental design and assisted in writing the manuscript. Allison Healey designed and conducted the penetration experiments in Fig. 3. Jonathan McMurry supervised Ms. Ngwa, designed and helped conduct biosensing experiments and was the principal author of the manuscript.

His coauthors also wish to acknowledge the contributions of John Salerno to their lives and careers. John was not only a colleague but a friend and mentor to us all. His passing is an irreplaceable loss but his presence in our lives is an invaluable blessing. We dedicate this paper to his memory.

Funding

This work was supported by National Institutes of Health grants GM102826 (to S.J.N.), GM111565 (to J.L.M.) and GM113522, National Science Foundation grant DBI-1229237 (to S.J.N. and J.C.S.), and by the Kennesaw State University Research & Services Foundation.

References

Abdiche, Y., Malashock, D., Pinkerton, A. and Pons, J. (2008). Determining kinetics and affinities of protein interactions using a parallel real-time label-free biosensor, the Octet. *Anal. Biochem.* **377**: 209-217.

Cardozo, A. K., Buchillier, V., Mathieu, M., Chen, J., Ortis, F., Ladriere, L., Allaman-Pillet, N., Poirot, O., Kellenberger, S., Beckmann, J. S., et al. (2007). Cell-permeable peptides induce dose- and length-dependent cytotoxic effects. *Biochim. et Biophys. Acta* **1768**(9).

Erazo-Oliveras, A., Muthukrishnan, N., Baker, R., Wang, T.-Y. and Pellois, J. (2012). Improving the endosomal escape of cell-penetrating peptides and their cargos: strategies and challenges. *Pharmaceuticals* **5**(1177-1209).

Fonseca, S. B., Pereira, M. P. and Kelley, S. O. (2009). Recent advances in the use of cell-penetrating peptides for medical and biological applications. *Adv. Drug Deliv. Rev.* **61**: 953-964.

Gautam, A., Singh, H., Tyagi, A., Chaudhary, K., Kumar, R., Kapoor, P. and Raghava, G. P. (2012). CPPsite: a curated database of cell penetrating peptides. *Database (Oxford)* **7**.

Gerber, N.C, and Ortiz de Montellano, P.R. (1995) Neuronal nitric oxide synthase. Expression in *Escherichia coli*, irreversible inhibition by phenyldiazene, and active site topology. *J. Biol. Chem.* **270**, 17791-17796.

Glogau, R., Blitzer, A., Brandt, F., Kane, M., Monheit, G. D. and Waugh, J. M. (2012). Results of a randomized, double-blind, placebo-controlled study to evaluate the efficacy and safety of a botulinum toxin type A topical gel for the treatment of moderate-to-severe lateral canthal lines. *J. Drugs Dermatol.* **11**(1): 38-45.

Green, M. and Lowenstein, P. M. (1988). Autonomous functional domains of chemically synthesized human immunodeficiency virus Tat trans-activator protein. *Cell* **55**: 1179-1188.

Hirose, H., Takeuchi, T., Osakada, Pujals, S., Katayama, S., Nakase, I., Kobayashi, S., Haraguchi, T. and Futaki, S. (2012). Transient focal membrane deformation induced by arginine-rich peptides leads to their direct penetration into cells. *Mol. Ther.* **20**(5): 984-993.

J**acobson, R. H., Zhang, X.-J., Dubose, R. F. and Matthews, B. W.** (1994). Three-dimensional structure of β-galactosidase from *E. coli*. *Nature* **369**: 761-766.

Johnson, R. M., Harrison, S. D. and Maclean, D. (2011). Therapeutic applications of cell-penetrating peptides. *Methods Mol. Biol.* **683**: 535-551.

Koren, E. and Torchilin, V. P. (2012). Cell-penetrating peptides: breaking through to the other side. *Trends Mol. Med.* **18**(7): 385-393.

Lonn, P. and Dowdy, S. F. (2015). Cationic PTD/CPP-mediated macromolecular delivery: charging into the cell. *Expert Opin. Drug Deliv.* **26**: 1-10.

Lundberg, M., Wikstrom, S. and Johansson, M. (2003). Cell surface adherence and endocytosis of protein transduction domains. *Mol. Ther.* **8**(1): 143-150.

McMurry, J. L., Chrestensen, C. A., Scott, I. M., Lee, E. W., Rahn, A. M., Johansen, A. M., Forsberg, B. J., Harris, K. D. and Salerno, J. C. (2011). Rate, affinity and calcium dependence of CaM binding to eNOS and nNOS: effects of phosphorylation. *FEBS J.* **278**(24): 4943-4954.

McMurry, J. L., Minamino, T., Furukawa, Y., Francis, J. W., Hill, S. A., Helms, K. A. and Namba, K. (2015). Weak interactions between Salmonella enterica FlhB and other flagellar export apparatus proteins govern type III secretion dynamics. *PLOS One* **10**(8): e0134884.

Palm-Apergi, C., Lonn, P. and Dowdy, S. F. (2012). Do cell-penetrating peptides actually "penetrate" cellular membranes? *Mol. Ther.* **20**(4): 695-697.

Roman, L.J., Sheta, E.A., Martasek, P., Gross, S.S., Liu, Q. and Masters, B.S. (1995) High-level expression of functional rat neuronal nitric oxide synthase in *Escherichia coli*. *Proc. Natl. Acad. Sci. USA*, **92**, 8428-8432.

Sebbage, V. (2009). Cell-penetrating peptides and their therapeutic applications. *Biosci. Horizons* **2**: 64-72.

Sultana, A. and Lee, J. E. (2015). Measuring protein-protein and protein-nucleic acid interactions by biolayer interferometry. *Curr. Protoc. Protein Sci.* **79**: 19.25.11-19.25-26.

Figures

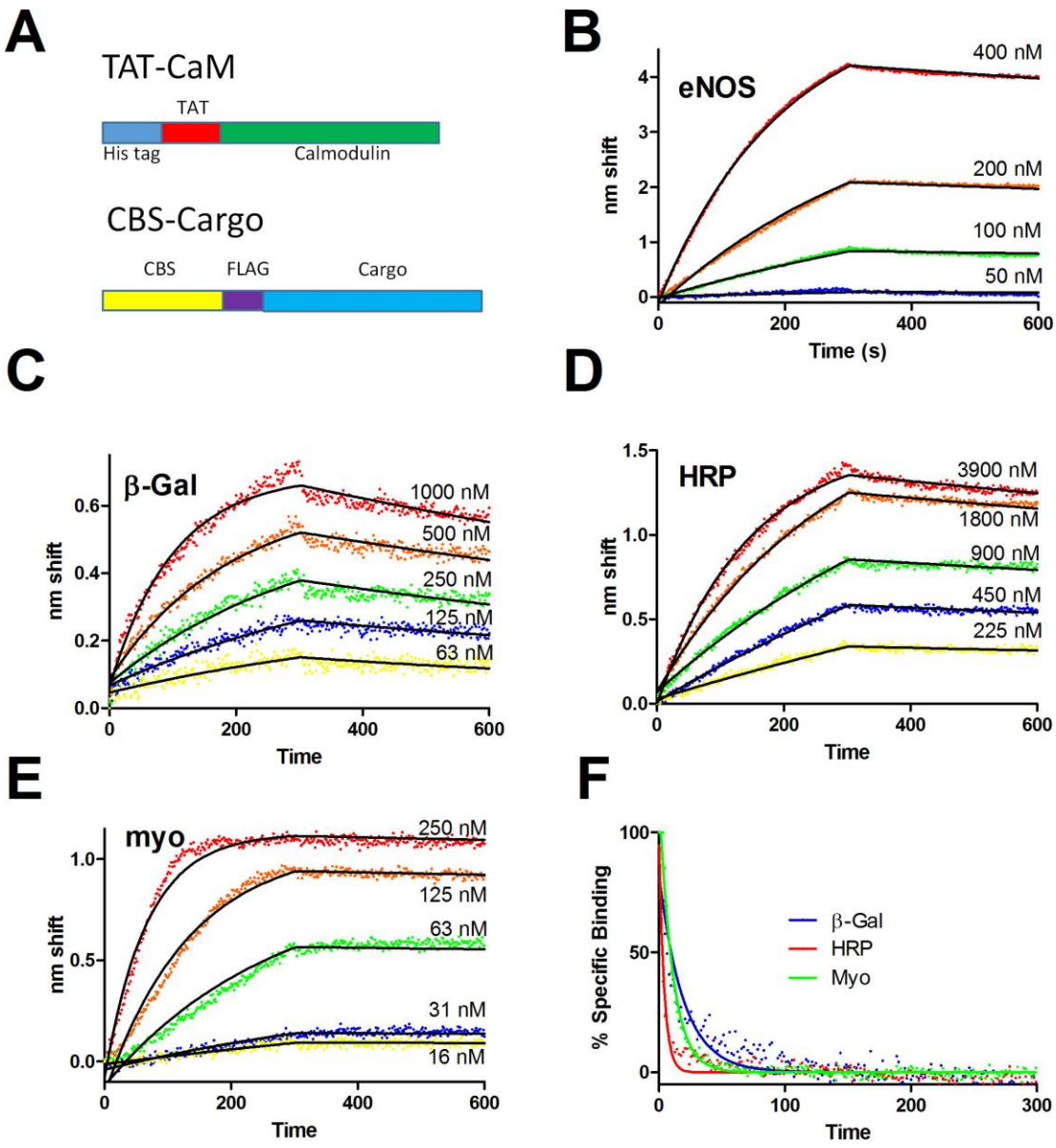

Figure 1. TAT-CaM cargo protein design and binding. (A) Schematic of TAT-CaM and cargo proteins with amino termini at left. (B-E) Biolayer interferometry (BLI) analysis of TAT-CaM

binding to (B) purified neuronal nitric oxide synthase. (C) CBS-β-Gal; (D) CBS-HRP; and (E) CBS-myoglobin. TAT-CaM was biotinylated and bound to streptavidin (SA) sensors. Reference-subtracted raw data are rendered as points with fits to a global single-state association-then-dissociation model. Analyte concentrations are noted for each trace. Association and dissociation phases were 300s in length. (F) After dissociation in buffer only, sensors were moved to buffer containing 10 mM EDTA. The rapid dissociation phases of the 1 µM samples for each cargo protein are shown. Binding is shown as % specific binding to reconcile the varying magnitudes of different analytes.

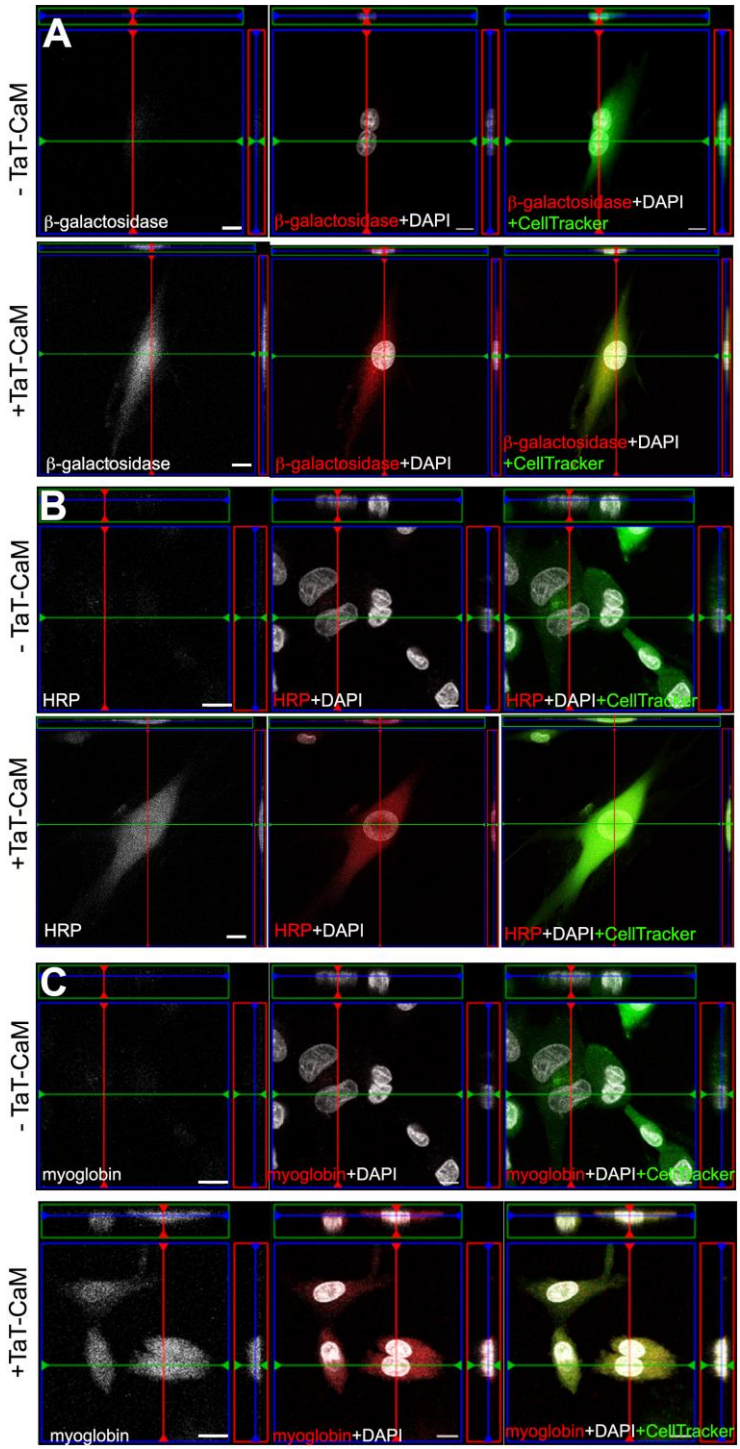

Figure 2. Confocal imaging of cell penetration. BHK cells were treated for 1 hour with DyLight 550 fluorescently labeled cargo proteins myoglobin (A), HRP (B) and B-Gal (C) (rendered as white in left panel, red in center and right panels), in either the absence or presence of TAT-CaM, washed and imaged live. Center images presented are optical sections set at a similar depth of the nucleus (NucBlue staining, white, center and right panel), as determined by position within the Z-stack. Orthogonal projections (boxed in red and green, respectively) are shown at the right and top sides of each panel. Cytoplasmic compartments in live cells were visualized using CellTracker Green CMFDA dye (green in right panel). Comparison of TAT-CaM-treated vs. untreated cells indicates that cargo proteins are entering into the cell, and are localized primarily to the cytoplasm. Scale bars in all panels = 20 μm. Each experiment was replicated at least twice with the same results.

Journal of Cell Science • Advance article

Figure 3. Cargo delivery occurs in various mammalian cell lines. HEK (A), and HT-3 (B) cells were treated for 1 hour with DyLight 550 fluorescently labeled CBS-myoglobin protein (white in left panel, red in center and right panels), in either the absence or presence of TAT-CaM, washed and imaged live. Orthogonal projections and center images that are optical sections set at a similar depth of the nucleus (NucBlue staining, white, right panel), as determined by position within the Z-stack are shown as in Fig. 2. Cytoplasmic compartments in live cells were visualized using CellTracker Green CMFDA dye (green in right panels). Comparison of TAT-CaM-treated vs. untreated cells indicates that cargo proteins are able to enter various mammalian cell types. Scale bars in all panels = 20 μm. These experiments were replicated once with the same results.

Tables

	K_D (nM)	k_{on} (M^{-1} s^{-1})	k_{off} (s^{-1})	k_{off} (EDTA) (s^{-1})
nNOS	15	1.2×10^4	$1.8 * 10^{-4}$	ND
β-Gal	73	9.2×10^3	$6.7 * 10^{-4}$	0.05
HRP	160	$1.7*10^3$	$2.8 * 10^{-4}$	0.2
Myo	0.9	5.9×10^4	$5.5 * 10^{-5}$	0.09

Table 1. Kinetic parameters for sensorgrams shown in Fig. 1. ND, not determined but previously reported to be ~0.1 s^{-1} (McMurry, et al., 2011).